Universität Karlsruhe (TH)
Institut für Baustatik

A Geometrical Nonlinear Brick Element based on the EAS–Method

S. Klinkel, W. Wagner

Mitteilung 5(1997)

Universität Karlsruhe (TH)
Institut für Baustatik

A Geometrical Nonlinear Brick Element based on the EAS–Method

S. Klinkel, W. Wagner

Mitteilung 5(1997)

Prof. Dr.–Ing. W. Wagner
Institut für Baustatik
Universität Karlsruhe
Postfach 6980
76128 Karlsruhe

Telefon: (0721) 608–2280
Telefax: (0721) 608–6015
E–mail: bs@.uni-karlsruhe.de
Internet: http://www.bs.uni-karlsruhe.de

A Geometrical Nonlinear Brick Element based on the EAS–Method

S.Klinkel and W.Wagner

1 Summary

This paper presents the development of a 3D brick element with enhanced assumed strains for a geometrically nonlinear theory. Some linear and nonlinear examples show that this element can be used successfully in the whole range of solid structures. Thin 2D – and 3D – beam and shell structures are calculated with few 3D elements and the results are the same as for shell and beam elements.

Keywords: 3D brick element, enhanced assumed strain, mixed finite element

2 Introduction

Low order plate, shell and volume elements are often preferred in structural mechanics. They can be used efficiently in nonlinear applications. Due to their simple geometry nearly every mesh generation program can be used. In many cases, especially in bending dominated problems, simple brick elements show severe stiffening effects known as locking. One possibility to overcome these phenomena is to derive elements from the Hellinger–Reissner principle. This principle bases on a hybrid–mixed method and contains independent stress– and displacement fields. An alternative way is to use the enhanced assumed strain (EAS) method described by Simo and Rifai [8]. In a geometrical linear theory the enhanced assumed strain method is identical to the Hellinger–Reissner method as shown by Andelfinger and Ramm in e.g. [1], [2]. This paper presents an enhanced assumed strain method in a geometrical nonlinear range. In reference [10] the good behavior of 3D enhanced elements in the nonlinear case was demonstrated. Here we want to show the applicability in the whole range of thin beam and shell structures without locking. In comparison to the standard Q1 elements the enhanced elements are especially in bending dominated problems very efficient.

We develop an 8–node solid element with independent interpolations for the stresses, strains and displacements. With respect to an orthogonality condition the stress field can be eliminated on the element level.

In the first section the variational formulation of a geometrical nonlinear theory with enhanced assumed strains will be presented. The basic idea of the EAS–method is to consider a strain field as the total sum of the compatible strains and the enhanced strains. Here the compatible part of the strains are the Green–Lagrangian strains and therefore we follow e. g. the approach of Betsch, Gruttmann and Stein [4].

Another strategy is to assume an enhanced displacement gradient within a spatial formulation, which has been presented by Simo and Amero [7].

To solve the system of nonlinear equations the Newton–Raphson method will be applied, which bases on the second variation of the potential.

Next we define the finite element approximation. In the compatible case we use simple displacement based isoparametric 3D elements. For the enhanced strains we define an interpolation matrix in isoparametric space (see also Simo and Rifai [8]). We choose an interpolation, which has been investigated for the infinitesimal theory by Andelfinger and Ramm [1]. This interpolation satisfies the patch test. Finally it is possible to map the interpolation matrix in physical space.

With the interpolation functions for the enhanced strains and for the compatible strains the consistent linearization of the weak form can be developed.

A variationally consistent recovery of the stress field from the nodal displacements has been presented for the infinitesimal theory by Simo and Rifai [8]. Based on the enhanced assumed Green–Lagrangian strains we extend it to the geometrical nonlinear case.

3 Variational formulation

The variational framework for the enhanced assumed strain method is the following three field variational functional in a Lagrangian description.

$$\Pi = \hat{\Pi}(\mathbf{u}, \tilde{\mathbf{E}}, \mathbf{S}) = \Pi_{int}(\mathbf{u}, \tilde{\mathbf{E}}, \mathbf{S}) + \Pi_{ext}(\mathbf{u}) \ . \tag{3.1}$$

The three independent variables are the displacement field $\mathbf{u}$, the enhanced strain field $\tilde{\mathbf{E}}$ and the second Piola Kirchhoff stress tensor $\mathbf{S}$. The idea of the EAS–method is to define the strains

$$\mathbf{E} := \underbrace{\mathbf{E}^c}_{\text{compatible}} + \underbrace{\tilde{\mathbf{E}}}_{\text{enhanced}} \tag{3.2}$$

as the total sum of the compatible $\mathbf{E}^c$ and enhanced $\tilde{\mathbf{E}}$ strains. The compatible part includes the terms for a geometrical nonlinear theory. Thus we introduce the Green–Lagrangian strain tensor

$$\mathbf{E}^c = \frac{1}{2}((\mathbf{1} + Grad\ \mathbf{u})^T(\mathbf{1} + Grad\ \mathbf{u}) - \mathbf{1}) \quad . \tag{3.3}$$

Based on the assumption that the material is homogeneous and hyperelastic the internal potential can be written as

$$\Pi_{int} = \int_{\mathcal{B}_0} W_{0S}(\mathbf{E}^c + \tilde{\mathbf{E}}) - \mathbf{S} : \tilde{\mathbf{E}} \quad dV \quad . \tag{3.4}$$

Where W_{0S} is the stored energy function of the initial reference configuration. The external potential for conservative external forces leads to

$$\Pi_{ext} = -\int_{\mathcal{B}_0} \rho_0 \bar{\mathbf{b}} \cdot \mathbf{u} \quad dV - \int_{\partial\mathcal{B}_0} \bar{\mathbf{t}} \cdot \mathbf{u} \quad dA \quad . \tag{3.5}$$

The first variation of the functional (3.1) at the point ($\mathbf{u}$, $\tilde{\mathbf{E}}$, $\mathbf{S}$) in the direction ($\delta\mathbf{u}$, $\delta\tilde{\mathbf{E}}$, $\delta\mathbf{S}$), denoted with $\delta\Pi$, is obtained via the directional derivative or the so-called Gâteaux derivation as

$$\delta\Pi = D\Pi(\mathbf{u}, \tilde{\mathbf{E}}, \mathbf{S}) \cdot (\delta\mathbf{u}, \delta\tilde{\mathbf{E}}, \delta\mathbf{S}) := \left. \frac{d}{d\varepsilon} \right|_{\varepsilon=0} \Pi(\mathbf{u}_\varepsilon \tilde{\mathbf{E}}_\varepsilon \mathbf{S}_\varepsilon) \quad . \tag{3.6}$$

Here the functions $\mathbf{u}_\varepsilon$, $\tilde{\mathbf{E}}_\varepsilon$, $\mathbf{S}_\varepsilon$ are defined by $\mathbf{u}_\varepsilon = \mathbf{u} + \varepsilon\delta\mathbf{u}$, $\tilde{\mathbf{E}}_\varepsilon = \tilde{\mathbf{E}} + \varepsilon\delta\tilde{\mathbf{E}}$ and $\mathbf{S}_\varepsilon = \mathbf{S} + \varepsilon\delta\mathbf{S}$. In the case of equilibrium the variation of the potential is

$$\delta\Pi = \frac{\partial\Pi(\mathbf{u} + \varepsilon\delta\mathbf{u})}{\partial\varepsilon} + \frac{\partial\Pi(\tilde{\mathbf{E}} + \varepsilon\delta\tilde{\mathbf{E}})}{\partial\varepsilon} + \frac{\partial\Pi(\mathbf{S} + \varepsilon\delta\mathbf{S})}{\partial\varepsilon} = 0 \quad . \tag{3.7}$$

With respect to the three independent variables we obtain

$$\begin{aligned} -\int_{\mathcal{B}_0} \delta\mathbf{S} : \tilde{\mathbf{E}} \quad dV &= 0 \\ \int_{\mathcal{B}_0} (\frac{\partial W_{0S}}{\partial \mathbf{E}} - \mathbf{S}) : \delta\tilde{\mathbf{E}} \quad dV &= 0 \\ \int_{\mathcal{B}_0} \frac{\partial W_{0S}}{\partial \mathbf{E}} : \delta\mathbf{E}^c \quad dV - \int_{\mathcal{B}_0} \rho_0 \mathbf{b}\, \delta\mathbf{u} \quad dV - \int_{\partial\mathcal{B}_0} \bar{\mathbf{t}}\, \delta\mathbf{u} dA &= 0 \end{aligned} \tag{3.8}$$

where $\delta\mathbf{E}^c$ denotes the variation of the compatible Green–Lagrangian strain tensor (3.2)

$$\delta\mathbf{E}^c = \frac{1}{2}(Grad^T \delta\mathbf{u}\ (1 + Grad\ \mathbf{u}) + (1 + Grad\ \mathbf{u})^T Grad\ \delta\mathbf{u}) \quad . \tag{3.9}$$

Standard arguments in the calculus of variations yield the following local Euler–Lagrange equations

$$\left.\begin{aligned} Div\ (\mathbf{FS}) + \rho_0\mathbf{b} &= 0 \\ \mathbf{S} &= \frac{\partial W_{0S}}{\partial \mathbf{E}} \\ \tilde{\mathbf{E}} &= 0 \end{aligned}\right\} \text{in } \mathcal{B}_0 \tag{3.10}$$

along with the natural boundary conditions

$$\bar{\mathbf{t}} = (\mathbf{FS})\ \mathbf{N} \qquad \text{on } \partial\mathcal{B}_0 \quad , \tag{3.11}$$

where $\mathbf{N}$ denotes the unit outward normal vector on $\partial\mathcal{B}_0$ and $\mathbf{F}$ is the deformation gradient tensor.

The system of nonlinear equations (3.8) can be solved by an iterative solution procedure. To obtain quadratic convergence for geometric nonlinear formulations the Newton–Raphson method can be used, which requires the consistent linearization of the first variation

$$\delta\Pi(\mathbf{u}_{k+1}, \tilde{\mathbf{E}}_{k+1}, \mathbf{S}_{k+1}) = \delta\Pi(\mathbf{u}_k, \tilde{\mathbf{E}}_k, \mathbf{S}_k) + D\delta\Pi(\mathbf{u}_k, \tilde{\mathbf{E}}_k, \mathbf{S}_k) \cdot (\Delta\mathbf{u}_{k+1}, \Delta\tilde{\mathbf{E}}_{k+1}, \Delta\mathbf{S}_{k+1}) = 0\ . \tag{3.12}$$

The directional derivative of the first variation of the potential is the second variation of the potential $\Delta\delta\Pi := D\delta\Pi(\mathbf{u}_k, \tilde{\mathbf{E}}_k, \mathbf{S}_k) \cdot (\Delta\mathbf{u}_{k+1}, \Delta\tilde{\mathbf{E}}_{k+1}, \Delta\mathbf{S}_{k+1})$. By straight forward computation the second variation has the following form:

$$\begin{aligned}
\Delta\delta\Pi \;=\; & \int_{\mathcal{B}_0} \delta\mathbf{E}^c \, \frac{\partial\partial W_{0S}}{\partial\mathbf{E}\partial\mathbf{E}} \, \Delta\mathbf{E}^c + \frac{\partial W_{0S}}{\partial\mathbf{E}} \, \delta\Delta\mathbf{E}^c \quad dV \;+\; \int_{\mathcal{B}_0} \delta\mathbf{E}^c \, \frac{\partial\partial W_{0S}}{\partial\mathbf{E}\partial\mathbf{E}} \, \Delta\tilde{\mathbf{E}} \quad dV \\
& + \int_{\mathcal{B}_0} \delta\tilde{\mathbf{E}} \, \frac{\partial\partial W_{0S}}{\partial\mathbf{E}\partial\mathbf{E}} \, \Delta\mathbf{E}^c \quad dV \;+\; \int_{\mathcal{B}_0} \delta\tilde{\mathbf{E}} \, \frac{\partial\partial W_{0S}}{\partial\mathbf{E}\partial\mathbf{E}} \, \Delta\tilde{\mathbf{E}} \quad dV \\
& - \int_{\mathcal{B}_0} \delta\mathbf{S} : \Delta\tilde{\mathbf{E}} \quad dV \;-\; \int_{\mathcal{B}_0} \delta\tilde{\mathbf{E}} : \Delta\mathbf{S} \quad dV \qquad .
\end{aligned} \tag{3.13}$$

4 Mixed finite element approximation

In this section we describe the finite element formulation for boundary value problems. We introduce a general finite element discretization constructed by isoparametric elements:

$$B^h = \mathop{\mathsf{A}}_{e=1}^{n_{elm}} B_e \tag{4.1}$$

Here A is the assembly operator for all elements n_{elm} and B_e is the volume of one element.

4.1 Compatible finite element interpolation

According to the isoparametric concept the standard isoparametric shape functions satisfy $N^A(\boldsymbol{\xi}_B) = \delta^A_B$ automatically. Here we use the standard trilinear shape functions for an eight node solid element, which approximate geometry and displacements. Consequently we can write

$$\mathbf{x}_e = \sum_{I=1}^{n_{nodes}} N_I \mathbf{x}_I \qquad \mathbf{u}_e = \sum_{I=1}^{n_{nodes}} N_I \mathbf{u}_I \quad . \tag{4.2}$$

Using vector notation and standard conventions in finite element analysis (see Zienkiewicz and Taylor [12]), it is possible to describe the first variation of the compatible Green–Lagrangian strain tensor

$$\delta\mathbf{E}^c_e = \sum_{I=1}^{n_{nodes}} \mathbf{B}_I \, \delta\mathbf{u}_I \; . \tag{4.3}$$

For a geometrical nonlinear theory the discrete strain operator $\mathbf{B}_I$ is a function of the displacements $\mathbf{u}$. Furthermore the discrete strain operator contains the derivatives of the shape functions N_I with respect to the global coordinates $\mathbf{x}$.

4.2 Interpolation of the enhanced strains

Next we introduce a formulation in isoparametric space for the enhanced strain interpolation. This formulation has to be transformed with the Jacobian matrix of the isoparametric map at the center of the element from isoparametric space into physical space. The enhanced strains are defined in the isoparametric domain as a rank two tensor, proposed by Simo and Rifai [8]

$$\tilde{\boldsymbol{\varepsilon}}_{\,kl} := \frac{det\mathbf{J}}{det\mathbf{J}_0}\, \mathbf{J}_{ki_0}\, \tilde{\mathbf{E}}_{ij}\, \mathbf{J}_{lj_0} \quad . \tag{4.4}$$

Here $\mathbf{J}$ denotes the Jacobian matrix and $\mathbf{J}_0$ is the Jacobian matrix at the center of the element

$$\mathbf{J}_0 = \left(\begin{array}{ccc} x_{,\xi} & y_{,\xi} & z_{,\xi} \\ x_{,\eta} & y_{,\eta} & z_{,\eta} \\ x_{,\zeta} & y_{,\zeta} & z_{,\zeta} \end{array} \right) \Bigg|_{\xi=0,\,\eta=0,\,\zeta=0} \quad . \tag{4.5}$$

The transformation (4.4) maps the enhanced strains in physical space $\tilde{\mathbf{E}}$ into the enhanced strains $\tilde{\boldsymbol{\varepsilon}}$ in isoparametric space. Using vector notation the inverse relation is given by

$$\tilde{\mathbf{E}}_e = \frac{det\mathbf{J}_0}{det\mathbf{J}}\, \mathbf{T}_0^{-T} \tilde{\boldsymbol{\varepsilon}}_{\,e} \quad . \tag{4.6}$$

The 6×6 matrix $\mathbf{T}_0$, already described e.g. by Andelfinger and Ramm [1], can be written as

$$\mathbf{T}_0 =$$

$$\left(\begin{array}{cccccc} J_{11_0}^2 & J_{21_0}^2 & J_{31_0}^2 & 2\,J_{11_0}J_{21_0} & 2\,J_{11_0}J_{31_0} & 2\,J_{21_0}J_{31_0} \\ J_{12_0}^2 & J_{22_0}^2 & J_{32_0}^2 & 2\,J_{12_0}J_{22_0} & 2\,J_{12_0}J_{32_0} & 2\,J_{22_0}J_{32_0} \\ J_{13_0}^2 & J_{23_0}^2 & J_{33_0}^2 & 2\,J_{13_0}J_{23_0} & 2\,J_{13_0}J_{33_0} & 2\,J_{23_0}J_{33_0} \\ J_{11_0}\,J_{12_0} & J_{21_0}\,J_{22_0} & J_{31_0}\,J_{32_0} & J_{11_0}\,J_{22_0} + J_{21_0}\,J_{12_0} & J_{11_0}\,J_{32_0} + J_{31_0}\,J_{12_0} & J_{21_0}\,J_{32_0} + J_{31_0}\,J_{22_0} \\ J_{11_0}\,J_{13_0} & J_{21_0}\,J_{23_0} & J_{31_0}\,J_{33_0} & J_{11_0}\,J_{23_0} + J_{21_0}\,J_{13_0} & J_{11_0}\,J_{33_0} + J_{31_0}\,J_{13_0} & J_{21_0}\,J_{33_0} + J_{31_0}\,J_{23_0} \\ J_{12_0}\,J_{13_0} & J_{22_0}\,J_{23_0} & J_{32_0}\,J_{33_0} & J_{12_0}\,J_{23_0} + J_{22_0}\,J_{13_0} & J_{12_0}\,J_{33_0} + J_{32_0}\,J_{13_0} & J_{22_0}\,J_{33_0} + J_{32_0}\,J_{23_0} \end{array} \right) . \tag{4.7}$$

Subsequently, we introduce a formulation for the enhanced strain field interpolation in isoparametric space. This interpolation matrix can be transformed via equation (4.6) into the global coordinates. First we note the interpolation relation on element level in vector notation

$$\tilde{\boldsymbol{\varepsilon}}_{\,e} = \mathbf{M}(\xi,\, \eta,\, \zeta)\, \boldsymbol{\alpha}_e \quad , \quad \boldsymbol{\alpha}_e \in \mathbb{R}^{n_\varepsilon} \quad . \tag{4.8}$$

Here $\boldsymbol{\alpha}$ is the vector of the internal strain parameters. The dimension of $\boldsymbol{\alpha}$ can be larger than the dimension of the enhanced strain vector. For the definition of

the interpolation matrix $\mathbf{M}(\xi,\,\eta,\,\zeta)$ we have to consider the orthogonality condition described by equation $(3.8)_1$. Choosing $\delta\mathbf{S}_e$ as an element–wise constant function $\delta\mathbf{S}_e^0$ for each element, condition $(3.8)_1$ implies

$$\int_{B_e} \delta\mathbf{S}_e^0 \cdot \tilde{\mathbf{E}}_e \, dV = 0 \quad . \tag{4.9}$$

With the transformation (4.6) we obtain

$$\int_{B_e} \delta\mathbf{S}_e^0 \, \frac{det\mathbf{J}_0}{det\mathbf{J}} \, \mathbf{T}_0^{-T} \, \tilde{\boldsymbol{\varepsilon}}_{\,e} \, det\mathbf{J} \, d\xi \, d\eta \, d\zeta = 0 \quad . \tag{4.10}$$

Here, the constant values $(\delta\mathbf{S}_e^0,\, det\mathbf{J}_0,\, \mathbf{T}_0^{-T})$ can be eliminated from this equation. Having in mind relation (4.8) the condition reduces to

$$\int_{B_e} \mathbf{M}(\xi,\,\eta,\,\zeta) \, \boldsymbol{\alpha}_e \, d\xi \, d\eta \, d\zeta = 0 \quad . \tag{4.11}$$

The interpolation matrix $\mathbf{M}$ has to satisfy this patch test (see also Simo and Rifai [8]). One possible interpolation matrix has been investigated for the infinitesimal theory by Andelfinger and Ramm [1]

$\mathbf{M} =$

$$\left(\begin{array}{ccc|cccccc|cccccc|cccccc|cccccc}
\xi & 0 & 0 & 0 & 0 & 0 & 0 & 0 & 0 & 0 & 0 & 0 & 0 & 0 & \xi\eta & \xi\zeta & 0 & 0 & 0 & 0 & 0 & 0 & 0 & \xi\eta\zeta & 0 & 0 & 0 & 0 & 0 \\
0 & \eta & 0 & 0 & 0 & 0 & 0 & 0 & 0 & 0 & 0 & 0 & 0 & 0 & 0 & 0 & \xi\eta & \eta\zeta & 0 & 0 & 0 & 0 & 0 & 0 & \xi\eta\zeta & 0 & 0 & 0 & 0 \\
0 & 0 & \zeta & 0 & 0 & 0 & 0 & 0 & 0 & 0 & 0 & 0 & 0 & 0 & 0 & 0 & 0 & 0 & \xi\zeta & \eta\zeta & 0 & 0 & 0 & 0 & 0 & \xi\eta\zeta & 0 & 0 & 0 \\
0 & 0 & 0 & \xi & \eta & 0 & 0 & 0 & 0 & \xi\zeta & \eta\zeta & 0 & 0 & 0 & 0 & 0 & 0 & 0 & 0 & 0 & \xi\eta & 0 & 0 & 0 & 0 & 0 & \xi\eta\zeta & 0 & 0 \\
0 & 0 & 0 & 0 & 0 & \xi & \zeta & 0 & 0 & 0 & 0 & \xi\eta & \eta\zeta & 0 & 0 & 0 & 0 & 0 & 0 & 0 & 0 & \xi\zeta & 0 & 0 & 0 & 0 & 0 & \xi\eta\zeta & 0 \\
0 & 0 & 0 & 0 & 0 & 0 & 0 & \eta & \zeta & 0 & 0 & 0 & 0 & \xi\eta & \xi\zeta & 0 & 0 & 0 & 0 & 0 & 0 & 0 & \eta\zeta & 0 & 0 & 0 & 0 & 0 & \xi\eta\zeta
\end{array}\right) . \tag{4.12}$$

The interpolation matrix expands the whole strain field up to a complete trilinear field. Finally, we can formulate the interpolation function for the enhanced strains $\tilde{\mathbf{E}}$ in physical space

$$\tilde{\mathbf{E}}_e = \mathbf{G}_E(\xi,\,\eta,\,\zeta) \, \boldsymbol{\alpha}_e \tag{4.13}$$

with

$$\mathbf{G}_E(\xi,\,\eta,\,\zeta) = \frac{det\mathbf{J}_0}{det\mathbf{J}} \, \mathbf{T}_0^{-T} \, \mathbf{M}(\xi,\,\eta,\,\zeta) \quad . \tag{4.14}$$

5 Consistent linearization of the discrete weak form

In this section the variational formulation will be described with the interpolation functions from section four.
First stresses and material law will be defined. We introduce a hyperelastic or Green–elastic material as a basis, so the elasticity–tensor is given by

$$\mathbb{C} = \frac{\partial \partial W_{0S}}{\partial \mathbf{E} \partial \mathbf{E}} \quad . \tag{5.1}$$

In view of the fact that the 2^{nd} Piola Kirchhoff stress tensor and the strain tensor $\mathbf{E}$ are symmetrical and W_{0S} has potential properties, the rank four elasticity tensor can be noted as a 6×6 matrix $\mathbb{C}$. In addition we define a stress field

$$\hat{\mathbf{S}} = \frac{\partial W_{0S}}{\partial \mathbf{E}} \tag{5.2}$$

with corresponding ordering of the components in vector notation

$$\hat{\mathbf{S}} = (S_{11}, S_{22}, S_{33}, S_{12}, S_{13}, S_{23})^T \quad . \tag{5.3}$$

Another aspect has been taken into account, the orthogonality condition between the discontinuous element stresses and the enhanced interpolations. With this condition, the 2^{nd} Piola Kirchhoff stress field is effectively eliminated from the variational equations (3.8) and (3.13). The three field variational formulation is reduced to a two field formulation

$$\begin{aligned}
&\int_{\mathcal{B}_0} -\hat{\mathbf{S}}\ \delta\tilde{\mathbf{E}} \quad dV + \int_{\mathcal{B}_0} \hat{\mathbf{S}}\ \delta\mathbf{E}^c \quad dV - \int_{\mathcal{B}_0} \rho_0 \mathbf{b}\ \delta\mathbf{u} \quad dV - \int_{\partial\mathcal{B}_0} \bar{\mathbf{t}}\ \delta\mathbf{u} \quad dV \\
&+ \int_{\mathcal{B}_0} \left(\delta\mathbf{E}^c\ \mathbb{C}\ \Delta\mathbf{E}^c + \hat{\mathbf{S}}\ \delta\Delta\mathbf{E}^c\right) \quad dV + \int_{\mathcal{B}_0} \delta\mathbf{E}^c\ \mathbb{C}\ \Delta\tilde{\mathbf{E}} \quad dV \\
&+ \int_{\mathcal{B}_0} \delta\tilde{\mathbf{E}}\ \mathbb{C}\ \Delta\mathbf{E}^c \quad dV + \int_{\mathcal{B}_0} \delta\tilde{\mathbf{E}}\ \mathbb{C}\ \Delta\tilde{\mathbf{E}} \quad dV \quad = \quad 0\,.
\end{aligned} \tag{5.4}$$

Substituting the virtual strains by the previous interpolations (4.3) and (4.13)

$$\begin{aligned}
\delta\mathbf{E}_e^c &= \sum_{I=1}^{n_{nodes}} \mathbf{B}_I\ \delta\mathbf{u}_I \\
\delta\tilde{\mathbf{E}}_e &= \mathbf{G}_E\ \delta\boldsymbol{\alpha}_e
\end{aligned} \tag{5.5}$$

in equation (5.4) yields the consistent linearization of the discrete weak form on element level

$$\begin{aligned}
\sum_{I=1}^{n_{nodes}} \delta\mathbf{u}_I^T \quad & \left(\int_{\mathcal{B}_e} \mathbf{B}_I^T \, \hat{\mathbf{S}} \, dV - \int_{\mathcal{B}_e} \mathbf{N}_I^T \, \rho_0 \mathbf{b} \, dV - \int_{\partial\mathcal{B}_e} \mathbf{N}_I^T \, \bar{\mathbf{t}} \, dA \right. \\
& \left. + \sum_{J=1}^{n_{nodes}} \int_{\mathcal{B}_e} (\mathbf{B}_I^T \, \mathbb{C} \, \mathbf{B}_J + \mathbf{G}_{IJ}) \, dV \, \Delta\mathbf{u}_J + \int_{\mathcal{B}_e} \mathbf{B}_I^T \, \mathbb{C} \, \mathbf{G}_E \, dV \, \Delta\boldsymbol{\alpha}_e \right) \\
+ \; \delta\boldsymbol{\alpha}_e^T \quad & \left(\int_{\mathcal{B}_e} \mathbf{G}_E^T \, \hat{\mathbf{S}} \, dV + \sum_{J=1}^{n_{nodes}} \int_{\mathcal{B}_e} \mathbf{G}_E^T \, \mathbb{C} \, \mathbf{B}_J \, dV \, \Delta\mathbf{u}_J + \int_{\mathcal{B}_e} \mathbf{G}_E^T \, \mathbb{C} \, \mathbf{G}_E \, dV \, \Delta\boldsymbol{\alpha}_e \right) = 0 \,.
\end{aligned} \tag{5.6}$$

The part $\int_{\mathcal{B}_e} \mathbf{G}_{IJ} \, dV$ is the initial stress matrix. With respect to the interpolations (4.2) it can conclude from equation $\int_{\mathcal{B}_0} \hat{\mathbf{S}} \, \delta\Delta\mathbf{E}^c \, dV$ (5.4).

Considering of equation (5.6) we point out the solution strategy for the general displacement problem $\mathbf{K}_T \, \Delta\mathbf{u} = \mathbf{R}$ in Table (5.1).

start values: $\boldsymbol{\alpha}_e^{(k+1)} = \mathbf{0}\ ,\ \mathbf{u}_e^{(k+1)} = \mathbf{0}$

1. compute internal and external forces

$$\mathbf{f}_{eI}^{\,int\,(k+1)} = \int_{\mathcal{B}_e} [\mathbf{B}_I^{(k+1)}]^T\ \hat{\mathbf{S}}(\mathbf{u}_e^{(k+1)}\,,\,\boldsymbol{\alpha}_e^{(k+1)}) \quad dV$$

$$\mathbf{f}_{eI}^{\,ext} = \int_{\mathcal{B}_e} \mathbf{N}_I^T\ \rho_0 \mathbf{b} \quad dV + \int_{\partial\mathcal{B}_e} \mathbf{N}_I^T\ \bar{\mathbf{t}} \quad dA$$

2. $\mathbf{R}_e = [\boldsymbol{\Gamma}_{\ e}^{(k+1)}]^T\ \mathbf{H}_e^{-1}\ \mathbf{h}_e^{(k+1)} + \mathbf{f}_e^{ext} - \mathbf{f}_e^{int\,(k+1)}$
   if $\mathbf{R} = \mathop{\mathbf{A}}_{e=1}^{n_{elm}} \mathbf{R}_e \leq$ tolerance $\rightarrow$ END

3. compute components of modified tangential stiffness matrix

$$\boldsymbol{\Gamma}_{\ eI}^{(k+1)} = \int_{\mathcal{B}_e} \mathbf{G}_E^T\ \mathbb{C}\ \mathbf{B}_I(\mathbf{u}_e^{(k+1)}) \quad dV$$

$$\mathbf{K}_{eIJ}^{(k+1)} = \int_{\mathcal{B}_e} \Big(\mathbf{B}_I^T(\mathbf{u}_e^{(k+1)})\ \mathbb{C}\ \mathbf{B}_J(\mathbf{u}_e^{(k+1)}) + \mathbf{G}_{IJ}(\mathbf{u}_e^{(k+1)})\Big) \quad dV$$

$$\mathbf{h}_e^{(k+1)} = \int_{\mathcal{B}_e} \mathbf{G}_E^T\ \hat{\mathbf{S}}(\mathbf{u}_e^{(k+1)}\,,\,\boldsymbol{\alpha}_e^{(k+1)}) \quad dV$$

$$\mathbf{H}_e = \int_{\mathcal{B}_e} \mathbf{G}_E^T\ \mathbb{C}\ \mathbf{G}_E \quad dV$$

4. assemble and solve

$$\mathbf{K}_T^{(k+1)} = \mathop{\mathbf{A}}_{e=1}^{n_{elm}} \mathbf{K}_e^{(k+1)} - [\boldsymbol{\Gamma}_{\ e}^{(k+1)}]^T\ \mathbf{H}_e^{-1}\ \boldsymbol{\Gamma}_{\ e}^{(k+1)}$$

$$\mathbf{R}^{(k+1)} = \mathop{\mathbf{A}}_{e=1}^{n_{elm}} [\boldsymbol{\Gamma}_{\ e}^{(k+1)}]^T\ \mathbf{H}_e^{-1}\ \mathbf{h}_e^{(k+1)} + \mathbf{f}_e^{ext} - \mathbf{f}_e^{int\,(k+1)}$$

$$\mathbf{K}_T^{(k+1)} \Delta\mathbf{u}^{(k+1)} = \mathbf{R}^{(k+1)}$$

5. update variables

$$\mathbf{u}_e^{(k+1)} = \mathbf{u}_e^{(k+1)} + \Delta\mathbf{u}_e^{(k+1)}$$

$$\boldsymbol{\alpha}_e^{(k+1)} = \boldsymbol{\alpha}_e^{(k+1)} - \mathbf{H}_e^{-1}(\mathbf{h}_e^{(k+1)} + \boldsymbol{\Gamma}_{\ e}^{(k+1)} \Delta\mathbf{u}_e^{(k+1)})$$

6. Go to 1

Table 5.1: Solution strategy

6 Stress recovery

Taking into account that the displacement field is known, we describe a function with the intention to minimize the stress error (see also Simo, Rifai [8])

$$L(\tilde{\mathbf{E}},\ \mathbf{S}) := \int_{\mathcal{B}_0} [\mathbb{C}(\mathbf{E}^c + \tilde{\mathbf{E}}) - \mathbf{S}] : \mathbb{C}^{-1} : [\mathbb{C}(\mathbf{E}^c + \tilde{\mathbf{E}}) - \mathbf{S}] dV \quad , \tag{6.1}$$

where $\tilde{\mathbf{E}}$, $\mathbf{S} \in R^{\tilde{E}} \times R^S$ and $\mathbf{u}$ are regarded as fixed. We claim that the least square minimization problem

$$L(\tilde{\mathbf{E}},\ \mathbf{S}) = MIN[L(\delta\tilde{\mathbf{E}},\ \delta\mathbf{S})] \tag{6.2}$$

defines the enhanced strain and stress field $(\tilde{\mathbf{E}},\ \mathbf{S})$. The first variation of $L(\tilde{\mathbf{E}},\ \mathbf{S})$ have to be zero, thus we obtain the following two independent equations:

$$\begin{aligned} \int_{\mathcal{B}_0} \delta\tilde{\mathbf{E}}[\mathbb{C}(\mathbf{E}^c + \tilde{\mathbf{E}}) - \mathbf{S}]\ dV &= 0 \\ \int_{\mathcal{B}_0} \delta\mathbf{S}[(\mathbf{E}^c + \tilde{\mathbf{E}}) - \mathbb{C}^{-1}\mathbf{S}]\ dV &= 0 \quad . \end{aligned} \tag{6.3}$$

In the last section we have defined $\hat{\mathbf{S}} = \frac{\partial W_{0S}}{\partial \mathbf{E}}$, thus we consider that $\frac{\partial W_{0S}}{\partial \mathbf{E}}$ is equal to $\mathbb{C}(\mathbf{E}^c + \tilde{\mathbf{E}})$. Inserting this results in equation $(3.8)_2$, we obtain that this equation is identical to $(6.3)_1$. In the case of balance the conditions (3.8) are satisfied, therefore we get the correct values of the enhanced strain parameters $\boldsymbol{\alpha}_e$. The second condition $(6.3)_2$ contains new information, from which we recover the stress field $\mathbf{S}$. First we have to choose an interpolation scheme for the element stresses $\mathbf{S}_e$

$$\mathbf{S}_e = \mathbf{G}_S \boldsymbol{\beta}_{\ e} \tag{6.4}$$

with

$$\mathbf{G}_S = \mathbf{T}_0 \mathbf{G}(\xi\,, \eta\,, \zeta) \quad . \tag{6.5}$$

The stress field $\mathbf{S}_e$ has to be orthogonal to the enhanced strain field $\tilde{\mathbf{E}}_e$. In view of equation $(3.8)_1$ we note

$$\int_{\mathcal{B}_0} \delta\boldsymbol{\beta}_{\ e}\ \mathbf{G}_S^T\, \mathbf{G}_E\ \boldsymbol{\alpha}_e\ det\mathbf{J}\ d\xi\, d\eta\, d\zeta = 0 \tag{6.6}$$

and with respect to equation (4.14) and (6.5) we obtain

$$\int_{\mathcal{B}_0} \mathbf{G}^T(\xi\,, \eta\,, \zeta)\ \mathbf{M}(\xi\,, \eta\,, \zeta)\ d\xi\, d\eta\, d\zeta = 0 \quad . \tag{6.7}$$

The interpolation matrix $\mathbf{G}$, which is orthogonal to $\mathbf{M}$ (4.12) has also been investigated by Andelfinger and Ramm [1]

$$\mathbf{G} = \begin{pmatrix} 1 & \eta & \zeta & \eta\zeta & 0 & 0 & 0 & 0 & 0 & 0 & 0 & 0 & 0 & 0 & 0 & 0 & 0 & 0 \\ 0 & 0 & 0 & 0 & 1 & \xi & \zeta & \xi\zeta & 0 & 0 & 0 & 0 & 0 & 0 & 0 & 0 & 0 & 0 \\ 0 & 0 & 0 & 0 & 0 & 0 & 0 & 0 & 1 & \xi & \eta & \xi\eta & 0 & 0 & 0 & 0 & 0 & 0 \\ 0 & 0 & 0 & 0 & 0 & 0 & 0 & 0 & 0 & 0 & 0 & 0 & 1 & \zeta & 0 & 0 & 0 & 0 \\ 0 & 0 & 0 & 0 & 0 & 0 & 0 & 0 & 0 & 0 & 0 & 0 & 0 & 0 & 1 & \eta & 0 & 0 \\ 0 & 0 & 0 & 0 & 0 & 0 & 0 & 0 & 0 & 0 & 0 & 0 & 0 & 0 & 0 & 0 & 1 & \xi \end{pmatrix} \quad . \tag{6.8}$$

Inserting equation (6.4) into $(6.3)_2$ yields in the sense of least square minimization the optimal stress field

$$\begin{aligned} \mathbf{S}_e &= \mathbf{G}_S \, \mathbf{H}_S^{-1} \, \mathbf{\Gamma}_S \\ \mathbf{H}_S &= \int_{\mathcal{B}_e} \mathbf{G}_S^T \, \mathbb{C}^{-1} \, \mathbf{G}_S \, det\mathbf{J} \, d\xi \, d\eta \, d\zeta \\ \mathbf{\Gamma}_S &= \int_{\mathcal{B}_e} \mathbf{G}_S^T \, \hat{\mathbf{E}}^c(\xi, \eta, \zeta) \, det\mathbf{J} \, d\xi \, d\eta \, d\zeta \quad , \end{aligned} \tag{6.9}$$

where $\hat{\mathbf{E}}^c$ are the strains evaluated for each Gausspoint ξ_P, η_P, ζ_P. These strains can be computed by

$$\hat{\mathbf{E}}^c(\xi, \eta, \zeta) = \frac{1}{2}[Grad \, \mathbf{u}^T Grad \, \mathbf{u} + Grad \, \mathbf{u}^T + Grad \, \mathbf{u}] \quad . \tag{6.10}$$

The operator $Grad \, \mathbf{u}$ is a function of ξ, η, ζ

$$Grad \, \mathbf{u} = \sum_{I=1}^{n_{nodes}} \begin{pmatrix} \mathbf{N}_{I,x} & 0 & 0 \\ 0 & \mathbf{N}_{I,y} & 0 \\ 0 & 0 & \mathbf{N}_{I,z} \\ \mathbf{N}_{I,y} & \mathbf{N}_{I,x} & \\ \mathbf{N}_{I,z} & 0 & \mathbf{N}_{I,x} \\ 0 & \mathbf{N}_{I,z} & \mathbf{N}_{I,y} \end{pmatrix} \mathbf{u}_I \quad . \tag{6.11}$$

7 Numerical examples

In this section we show the general applicability of enhanced eight node solid elements for thin beam and shell structures in several linear and nonlinear examples. The derived element has been implemented in an enhanced version of the program **FEAP**, documented in Zienkiewicz and Taylor [12].

7.1 Cooks membrane problem

The first example is used to test the correct EAS–formulation in the 2D case. Here we use the membrane problem defined by Cook [6], which is a popular two dimensional element test. Geometry and material data are given in Fig. 7.1. In Table 7.1 we note the relative vertical displacement of the top of the membrane for the standard Q1–element and for the enhanced Q1/E30–element. The reference solution is computed based on a 32x32 mesh.

mesh	2x2	4x4	8x8	16x16
Q1	0.466	0.732	0.904	0.971
Q1/E30	0.849	0.952	0.983	0.995

Table 7.1: Relative displacement of the top

In the geometric linear test the very good behavior of the enhanced elements is obvious. In comparison with the standard element the enhanced element shows nearly no locking as can be seen in Fig. 7.1. Basically, we obtain with the enhanced volume elements the same results as Andelfinger with enhanced shell elements.

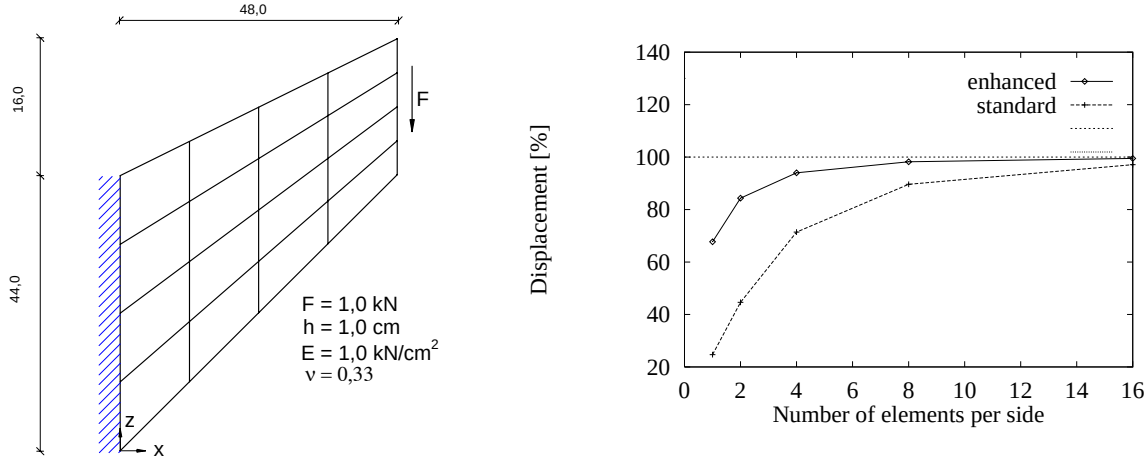

Figure 7.1: Cook's membrane problem

Next we investigate the Cooks membrane to demonstrate the difference in the stress recoveries. Within a geometrical nonlinear theory we compute the stresses at the fixed support. Therefore we use the first component $\mathbf{P}_{xx}$ of the 1. Piola–Kirchhoff stresses. All computations are carried out with enhanced 3D volume elements.

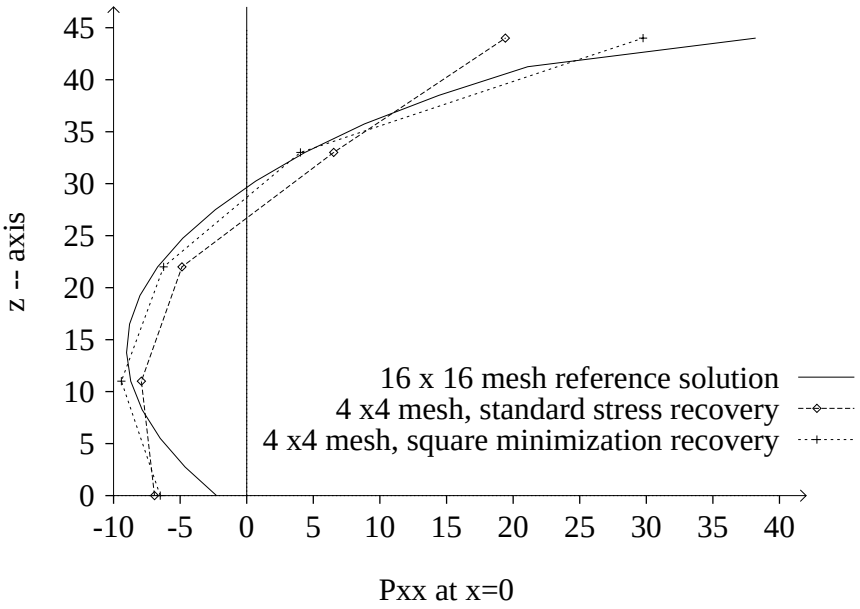

Figure 7.2: Stress result over the height at the support of the cooks membrane

The reference stress result is calculated with a 16 to 16 element mesh with one element in thickness direction. The other two curves base on a mesh with 4 elements over the height/length and one element over the thickness. It is obvious that the variational consistent stress recovery based on the square minimization problem produces much better stress results than the standard stress recovery via the material low.

7.2 Distortion test

Next we test the geometrical linear description of problems in the case of distorted meshes. A cantilever will be idealized with two elements, see Fig. 7.3. This mesh will be more and more distorted; the variable s is a parameter of the distortion.

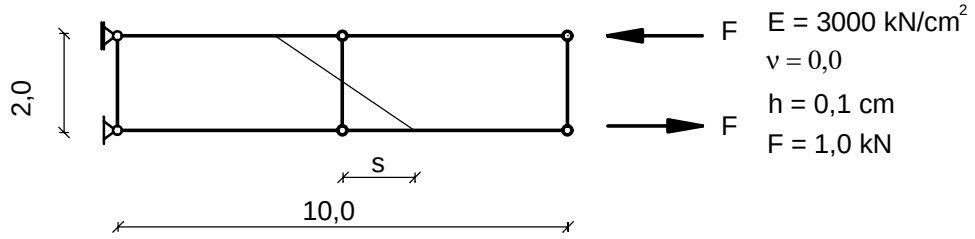

Figure 7.3: Distorted mesh

Fig. 7.4 shows the vertical displacement of the top of the cantilever with respect to the distortions. A reduction of the displacement is observed with increasing distortion of the mesh.
In particular the displacement of the standard Q1 element tends against zero, whereas the displacement of the enhanced Q1/E30 element has values about 50 % of the undistorted solution . The result of the 3D enhanced element is basically the same as in the investigation of Andelfinger and Ramm [1]. Better results can be obtained if the enhanced strains are interpolated with quadratic functions, see also [8] and [10].

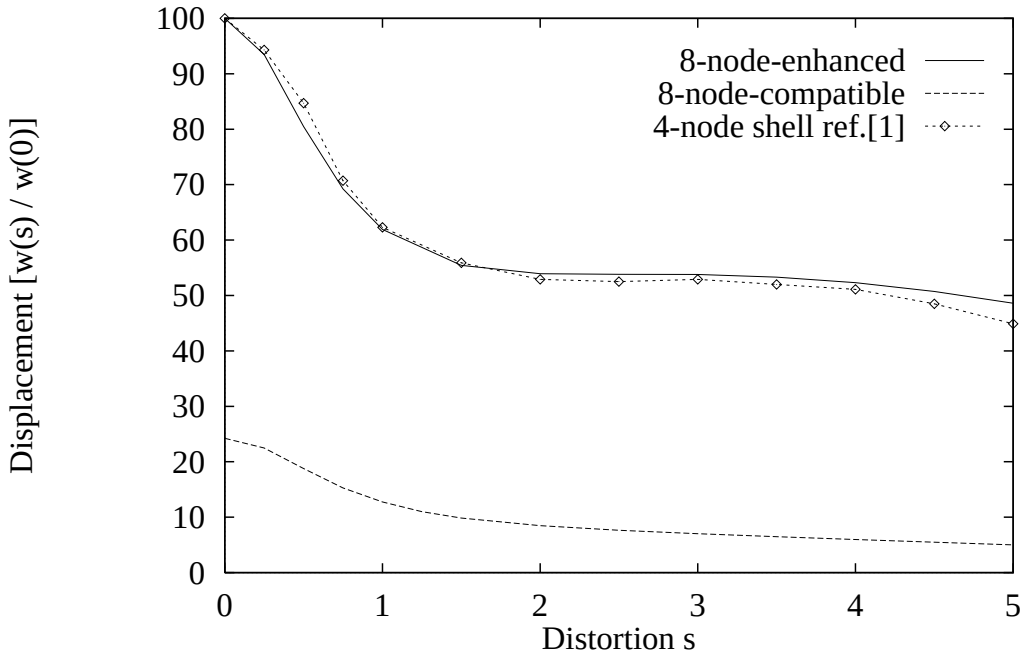

Figure 7.4: Displacement w of the distorted mesh

7.3 A 45–degree circular cantilever

The following example shows the applicability for thin 3D–beams. A 45–degree bend cantilever is provided with a concentrated end load as introduced by Bathe, Bolourchi [3], who used a sixteen-node solid element and by Slavkovic, Zivkovic,Kojic [10], who used an enhanced three-dimensional element. The large displacement response will be calculated for different vertical tip loads. The bend has a radius of 100 cm and a cross section of 1 to 1 cm, as illustrated in Fig. 7.5. The cantilever was discretized using 16 enhanced solid elements.

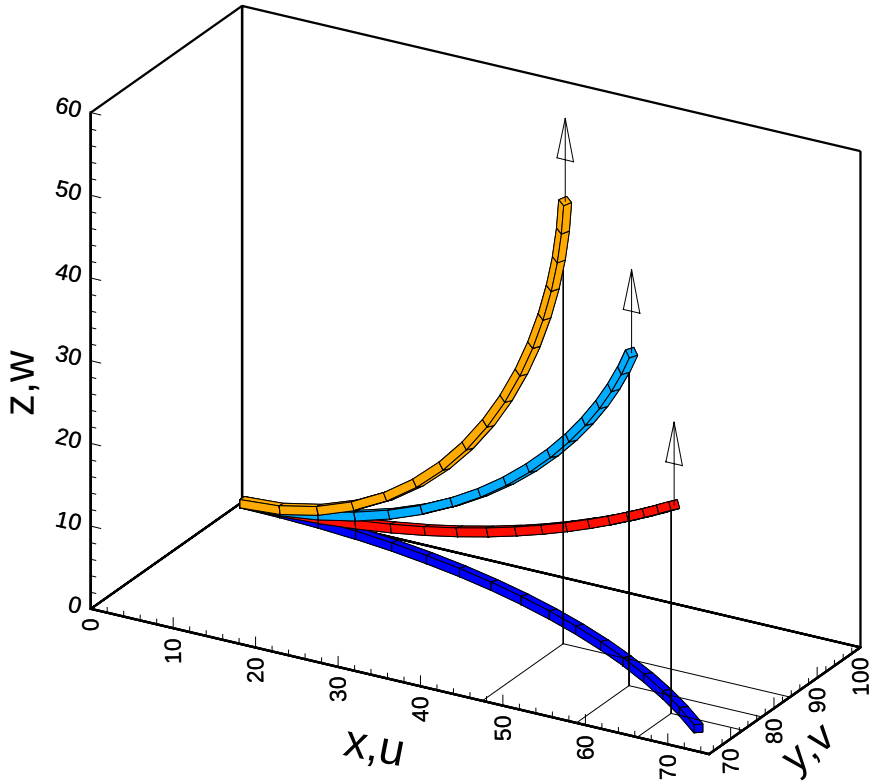

$E = 10^6\ N/cm^2$
$\nu = 0$

Figure 7.5: Circular cantilever under tip load of 150, 300 and 600 N

Fig. 7.6 presents the tip displacements for different load steps. For the load steps of 300 and 600 N we obtain exactly the same results as Slavkovic et.al. [10] .

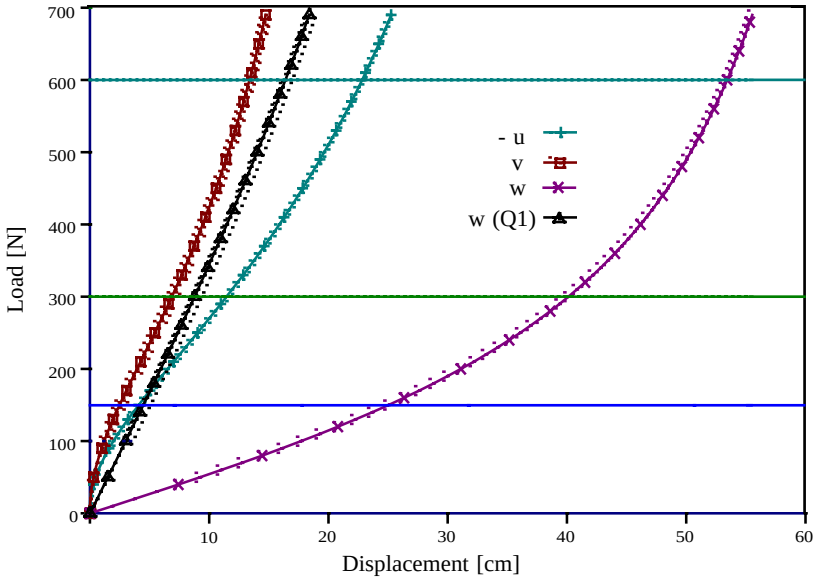

Figure 7.6: Load–deflection curve of the circular cantilever

7.4 A flat cylindrical segment

Now we discuss the modeling of shell structures with solid elements. We investigate the buckling behaviour of a flat cylindrical shell with a single point load. With respect to the symmetry (see Fig. 7.7) it is only necessary to discretize one quarter of the segment. The problem was idealized using 4 x 4 eight node solid elements in plane and 2 elements over the thickness to model the boundary conditions correctly, which are simply supported at the straight edges and free at the curved edges.

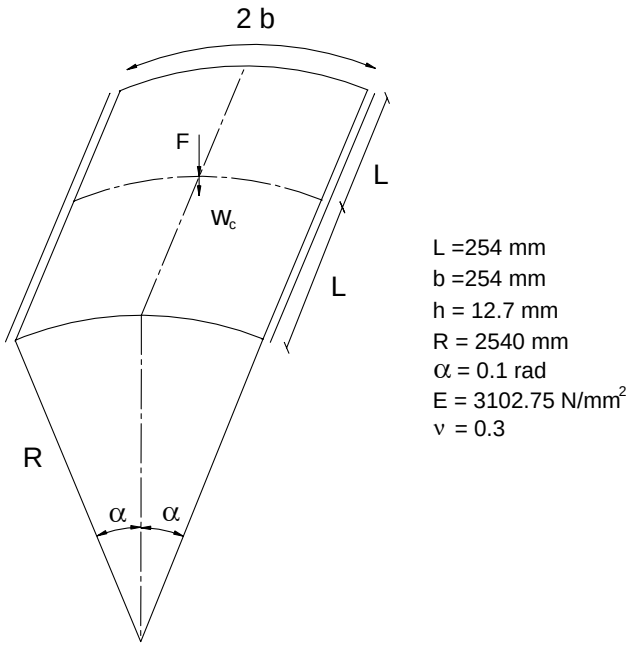

Figure 7.7: Flat cylindrical segment

In Fig. 7.8 the load–displacement curve of the enhanced 3D element and the compatible 3D element are depicted. It is obvious, that the compatible element is not able to describe the buckling phenomenon.

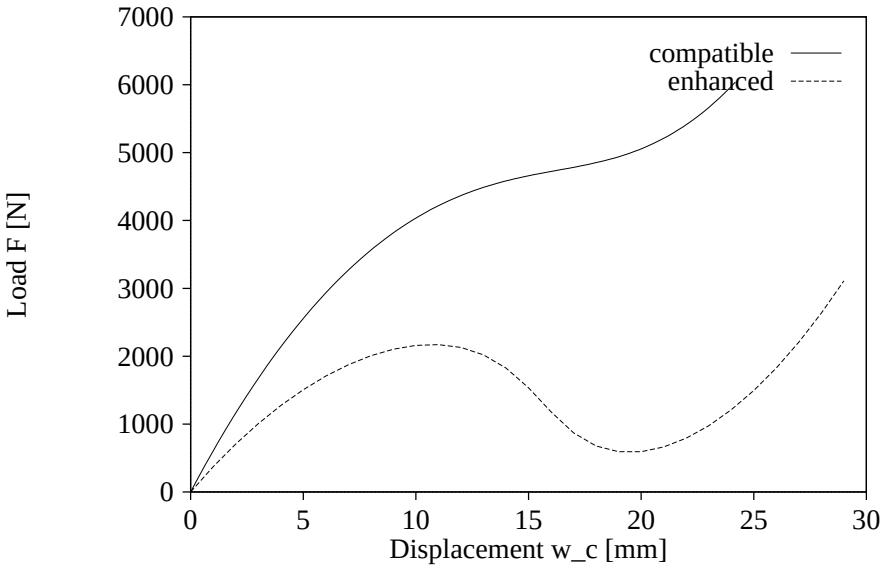

Figure 7.8: Load–deflection curve of the cylinder segment

In Table 7.2 the displacements for different load steps are shown. In comparison with the three dimensional elements, the solutions of a 4–node shell element, e.g. [11], are presented. Its obvious that the enhanced– and the shell–element leads nearly to the same results.

w_c in mm	3D compatible	3D enhanced	4–node shell element
2	1.161	0.706	0.730
4	3.135	1.273	1.315
6	2.931	1.707	1.760
8	3.561	2.007	2.066
10	4.035	2.160	2.221
12	4.367	2.129	2.189
14	4.583	1.827	1.876
16	4.723	1.180	1.178
18	4.853	0.677	0.654
20	5.057	0.592	0.782

Table 7.2: Load F in kN for different displacements w_c

7.5 A circular arch under single load

The next example shows the efficient use of the 3D element for a 3D beam problem with large displacements and stability behaviour. We consider an unsymmetrically supported circular arch under a vertical point load at the top, see Fig. 7.9. The finite element mesh consists of 30 enhanced 3–D elements with only one element for the whole cross section.

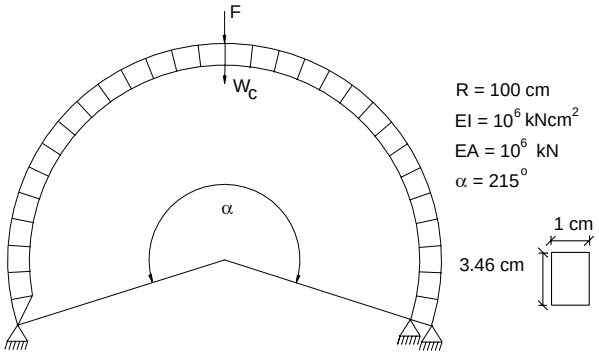

Figure 7.9: FE–mesh of the circular arch

In comparison with the 3D element, we compute this problem with 20 nonlinear beam elements, see also [9], [11]. In Fig. 7.10 the load–displacement curves for both approximations are given. Obviously it is possible to compute complicated nonlinear beam problems with enhanced volume elements. The good correspondence between the curves of the different FE–models is shown in Fig. 7.10.

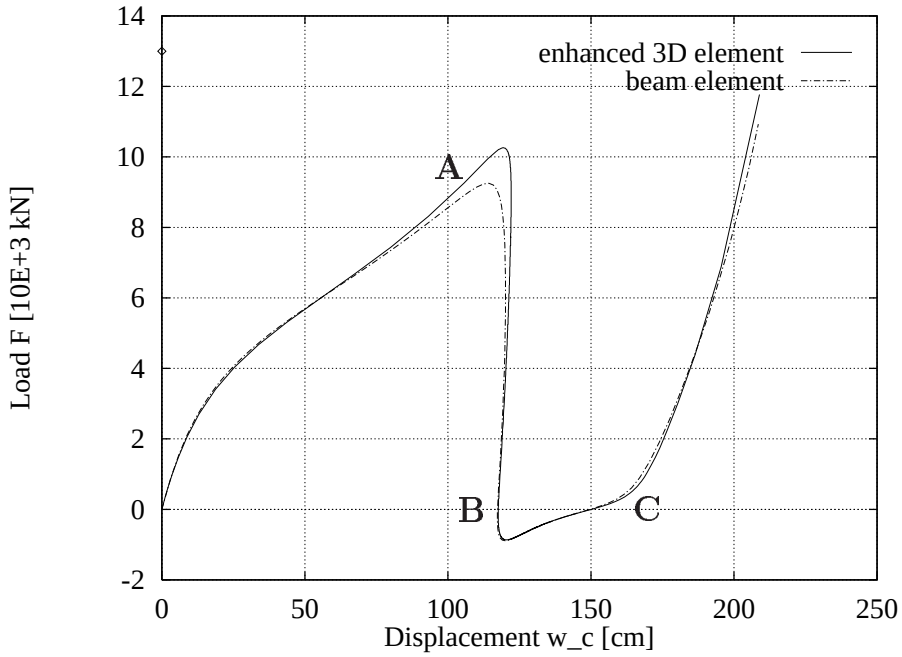

Figure 7.10: Load–displacement curves of the circular arch

Fig. 7.11 presents the deformed mesh for the points A, B and C. It should be noted that the structure penetrates the right support for large displacements, which is physically impossible.

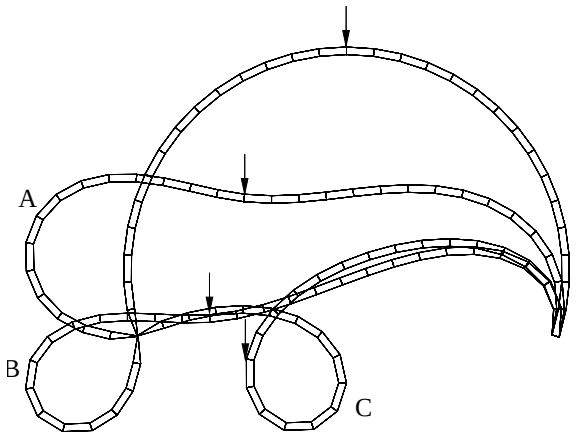

Figure 7.11: Deformed states of circular arch

7.6 Channel section beam

The last example demonstrates the applicability to thin shell structures with local stability effects, which demands a high accuracy of the chosen FE–model. The cantilever channel section beam load with a tip force at the free end has been previously investigated with shell elements in [5] and [4]. The geometry, the material data and the chosen finite element mesh are shown in Fig. 7.12. We idealize the channel section beam using 10x36 enhanced volume elements, with 10 elements in width/height– and 36 elements in length direction and again only 1 element in thickness direction.

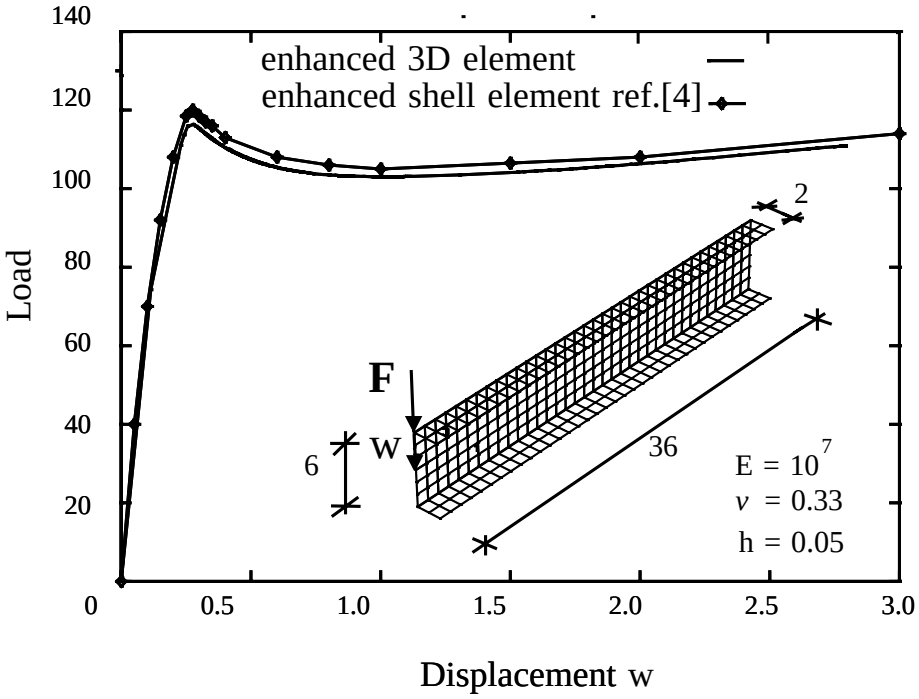

Figure 7.12: Load–deflection curve of the channel section beam

In the case of a nonlinear calculation the load–deflection curve (Fig. 7.12) is evaluated for the displacement w under the load F. For comparison, we note in the diagram the results of Betsch, Gruttmann and Stein [4], based on an enhanced geometric nonlinear shell element.

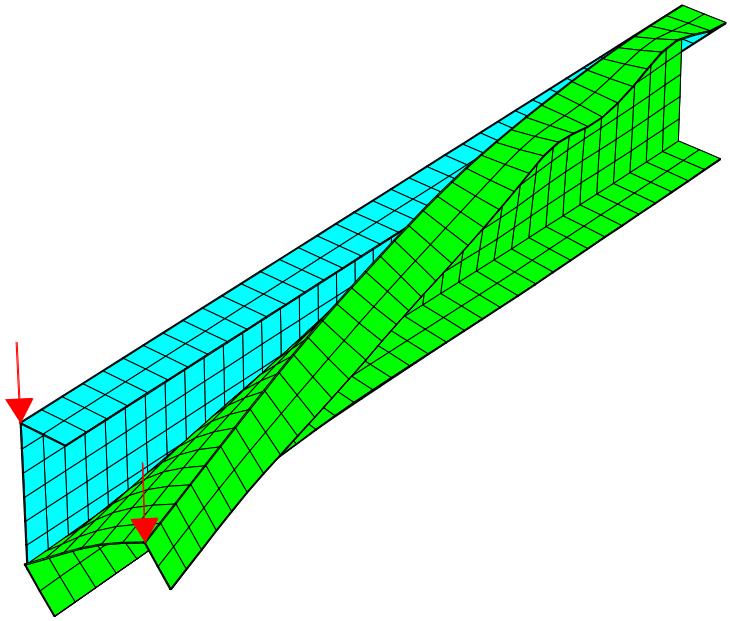

Figure 7.13: Deformed channel section beam

Fig. 7.13 shows the deformed mesh at the final state for a tip load of 110.9. The associated displacement of the point under the force in load direction is 2,79267. We obtain local buckling phenomena using the enhanced volume elements as well as using enhanced shell elements.

In this example the very good agreement between the solution of shell elements and the enhanced volume element is also obvious.

8 Concluding remarks

In this paper the derivation of a simple 3D brick element with enhanced shape functions for the strains has been developed. The examples show the applicability in the whole geometrically nonlinear range of thin beam and shell structures including stability effects. With few 3D brick elements the same results are obtained, as with beam or shell elements.

References

[1] Andelfinger, U. / Ramm, E.: *EAS-Elements for Two-Dimensional, Three-Dimensional, Plate and Shell Structures and their Equivalence to HR-Elements.* Int. J. Num. Meth. Eng. **36**, 1311–1337 (1993).

[2] Andelfinger, U. / Ramm, E. / Roehl, D.: *2D- and 3D- enhanced assumed strain elements and their application in plasticity.* In: Onate, E. / Owen, D.R.J., (Ed.), *Proc. 3rd Int. Conference on Computational Platicity Fundamentals and Applications*, Pineridge press, Swansea, 1992 .

[3] Bathe, Bolourchi: *Large displacement analysis of three-dimensional beam structures.* Int. J. Num. Meth. Eng. **14**, 961–986 (1979).

[4] Betsch, P. / Gruttmann, F. / Stein, E.: *A 4-node finite shell element for the implementation of general hyperelastic 3D-elasticity at finite strains.* Comp. Meth. Appl. Mech. Eng. **130**, 57–80 (1996).

[5] Chroscielewski, J. / Makowski, J. / Stumpf, H.: *Genuinely Resultant Shell Finite Elements Accounting For Geometric And Material Non–Linearity.* Int. J. Num. Meth. Eng. **35**, 63–94 (1992).

[6] Cook, R.D. / Asce, M.: *Improved Two- Dimensional Finite Element.* Journal of Structural Engineering **8**, 1851–1863 (1974).

[7] Simo, J.C. / Armero, F. / Taylor, R.L.: *Improved versions of assumed enhanced strain tri-linear elements for 3D finite deformation problems.* Comp. Meth. Appl. Mech. Eng. **110**, 359–386 (1993).

[8] Simo, J.C. / Rifai, D.: *A Class Of Mixed Assumed Strain Methods And The Method Of Incompatible Modes.* Int. J. Num. Meth. Eng. **29**, 1595–1638 (1990).

[9] Simo, J.C. / Wriggers, P. / Schweizerhof, K.H. / Taylor, R.L.: *Finite deformation post-buckling analysis involving inelasticity and contact constraints.* Int. J. Num. Meth. Eng. **23**, 779–800 (1986).

[10] Slavkovic, R. / Zivkovic, M. / Kojic, M.: *Enhanced 8-node three-dimensional solid and 4-node shell elements with incompatible generalized displacements.* Comm. Appl. Num. Meth. **10**, 699–709 (1994).

[11] Wagner, W.: *Stability Analysis of Shells with the Finite Element Method.* In: Rammerstorfer, F., G., (Ed.), *Nonlinear Analysis of Shells by Finite Elements*, Springer, Wien–New York, 1992.

[12] Zienkiewicz, O. C. / Taylor, R. L.: *The Finite Element Method.* Vol. I, McGraw-Hill, London, 4th ed., 1989.

List of Figures

List of Tables